IOP Conf. Series: Materials Science and Engineering **174** (2017) 012029 doi:10.1088/1757-899X/174/1/012029

Analysis of the bending stiffness and adhesion effect in RF-MEMS structures

C Birleanu[1], M Pustan[1], C Dudescu[2], V Merie[3] and I Pintea[1]

[1]Mechanical Systems Engineering Department, Technical University of Cluj-Napoca, Blv. Muncii no. 103-105, 400641, Cluj-Napoca, Romania
[2]Mechanical Engineering Department, Technical University of Cluj-Napoca, Blv. Muncii no. 103-105, 400641, Cluj-Napoca, Romania
[3]Materials Science and Engineering Department, Technical University of Cluj-Napoca, Blv. Muncii no. 103-105, 400641, Cluj-Napoca, Romania

E-mail: Corina.Barleanu@omt.utcluj.ro

Abstract. Microelectromechanical system (MEMS) is a special branch with a wide range of applications in sensing, switching and actuating devices. Designing the reliable MEMS for thin free-standing structures like as bridges and cantilevers requires understanding of the tribomechanical properties of the materials and structures.
The effect of geometrical dimensions (cross-section dimensions and length) on mechanical and tribological behavior of free-standing MEMS structures made of electroplated gold was analyzed in this paper. Special attention was given to the dependences between stiffness and cantilever length and the dependences between bending stress and variable travel range of actuated load. The force position was moved from the beams free-end toward to the anchor. The tests were performed at room temperature (22°C) and relative humidity RH of 40% with a noise- and vibration-isolated and environment-controlled XE-70 AFM from Park Systems using the contact mode. Each measurement was repeated many times in order to improve the accuracy of the experimental results. The stiffness of a microcantilever varies if the position of the acting force is changed. The experimental results obtained were in good correlation with those obtained analytically.

1. Introduction

Microelectromechanical systems (MEMS) are integrated electromechanical system where the components size and the actuating range are within the limits to micro-scale. Nowadays, due to increasingly mature process technology, several micro structural and functional sophisticated modules are available. Among the current MEMS devices, multiple MEMS devices are driven electrostatic such as capacitive pressure sensors, micro pumps, radio frequency (RF) switches, vacuum resonators etc. Electrostatic-driven MEMS devices have advantages of quick response, lower power consumption, and standard integrated circuit process compatibility [1]. One of the fundamental issues in building MEMS is scale effect [2]. In MEMS devices where size effects become prevalent determine different properties which deviate from their bulk characteristics. This leads to a grey area regarding the application of specific characterization technologies.

For the microcomponents from thin films is evident that stress-strain relationship is affected by the relatively high area to volume ratio. As a result, typical properties used for description of bulk material strength and deformation do not apply for thin films and micro devices. In particular, this size effect

relationship is not yet well understood when structural dimensions decrease from millimeters to micro and nanometers [1].

RF-sensors have been a subject of interest in recent years [3]. These sensors with high sensitivity to applied force, high resolution, low power consumption and digital output are an attractive alternative to conventional piezoresistive sensors.

The effect of geometrical dimensions on stiffness, stress and adhesion force of clamp-free MEMS structures (microcantilevers) is analysed in this work. Experimental investigations are performed on samples fabricated from gold with different geometrical dimensions using Atomic Force Microscope. For soft cantilevers, such as those employed in atomic force microscopy, the bending sensitivity can approach a few tenths of a newton per meter [4].

Microcantilever deflection is most commonly measured by reflecting a laser from the free end of the cantilever. An AFM cantilever experiences a point load at its free end (where the probe tip is located), whereas a cantilever with a functional coating for sensing applications experiences a distributed surface stress. Stress distribution in MEMS deformable component is changed depending on the contact areas between the flexible plate and the substrate. In this paper it is worth to discuss the overall influence of length scale on the performance of mechanical devices.

2. Theoretical considerations

2.1. Stiffness and stress

Electrostatic actuation and sensing are largely utilized in MEMS transducers due to advantages such as sensitivity, fast response, precision, relatively easy fabrication. It is well known that the flexible plate displacement of an electrostatic actuated MEMS resonator depends on the applied load.

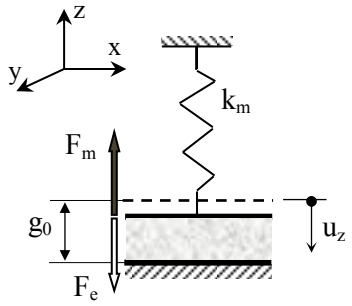

Figure 1. Model of a flexible parallel-plate system.

The maximum gap g_0 between the fixed and the mobile plates, initially occurs for $u_z = 0$ (figure 1). The static equilibrium sets in situation when the two opposing forces, the electrostatic force F_e and the spring force F_m, are equal:

$$F_e = F_m \tag{1}$$

The force produced through transverse electrostatic actuation is given by [2]:

$$F_e = \frac{\varepsilon \cdot A \cdot U^2}{2(g_0 - u_z)^2} \tag{2}$$

where: ε is the electric permittivity; A - overlapped area; U - the actuation voltage); g_0 - the initial gap in the z direction; u_z - the displacement produced through attraction electrostatic forces.

The spring (mechanical) force F_m is:

$$F_m = k_m \cdot u_z \tag{3}$$

where k_m is the spring constant.

When the electrostatic force F_e is larger than the mechanical force F_m given by the spring constant, the system becomes unstable. In this way for displacements larger than one-third of the initial gap (pull-in position), the mobile plate collapses against the fixed one [5].

The main failure cause in MEMS is stiction when the flexible plate collapses into nearby surfaces, resulting in their permanent adhesion. This situation can arise either during fabrication or operation. Under stiction the contact area between flexible plate and substrate increases if the applied load increases, respectively. The cantilevers with rectangular cross-sections under investigation are subjected to a mechanical force applied in the position 1 on samples as presented in figure 2. In the first case, the force is applied at the cantilever free- end. Then, the force is moved toward to the beam

anchor. In both situations the investigated cantilevers are bending directly to substrate. The cantilevers of rectangular cross-sections under our investigation have the configuration (*w* - width, *t* - thickness and *l* - length) as presented in figure 3 and are subjected to a force *F*.

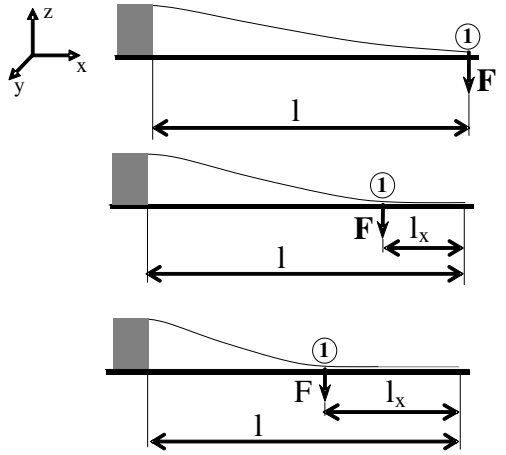

Figure 2. Bending of a microcantilever to substrate for different force positions [6, 8].

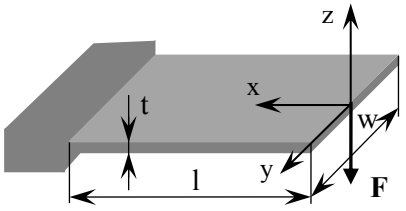

Figure 3. Microcantilever subjected to a mechanical force.

The stiffness and stress in beam is changed when the position of the applied force which bends the flexible plate to substrate, is moved towards to the anchor. As a consequence, two situations should be considered in our study. First, for long beams when the distance $(l-l_x)$ is at least 5 times larger than the largest cross-sectional dimension when the cross-sections remain perpendicular to the neutral axis during displacement and the Euler-Bernoulli beam model is used [5].

Secondly, for relatively-short distance $(l-l_x)<5w$, shearing effects become important, and the regular bending deformations are augmented by the addition of shearing deformations, according to the Timoshenko's beam model. In this case, the cross-sections are no longer perpendicular to the neutral axis in the deformed state [5]. Corresponding to this situation, when the shearing effects become important, normal and tangential stresses are produced simultaneously in flexible plates.

If $(l-l_x)\geq 5w$, the deflection at the point 1 of the microcantilever (figure 2) can be determined as:

$$u_{1z} = F \cdot \frac{(l-l_x)^3}{3E \cdot I_y} \tag{4}$$

where I_y is the axial moment of inertia and E is the longitudinal modulus of elasticity.

The z-direction stiffness of the microcantilever is:

$$k = \frac{3E \cdot I_y}{(l-l_x)^3} \tag{5}$$

The bending stress appearing in cantilever can be analytically computed as:

$$\sigma_b = \frac{6F \cdot (l-l_x)}{w \cdot t^2} \tag{6}$$

If the force is applied at a distance $(l-l_x)<5w$, the stiction area is large and shearing effects became important. The deflection and force dependence is given by the relation:

$$u_{1z} = F \cdot (l-l_x) \cdot \left[\frac{(l-l_x)^2}{3EI_y} + \frac{\kappa}{GA} \right] \tag{7}$$

where A is the cross-sectional area, G is the shear modulus and $\kappa = 6/5$ for rectangular cross-sections from Young and Budynas [7].

Based on shearing effect the stiffness of cantilever $k_{(sh)}$ could be expressed by [5]:

$$k_{(sh)} = \frac{3E \cdot G \cdot I_y \cdot A}{(l - l_x)\left[G \cdot A \cdot (l - l_x)^2 + 3\kappa \cdot EI_y\right]} \tag{8}$$

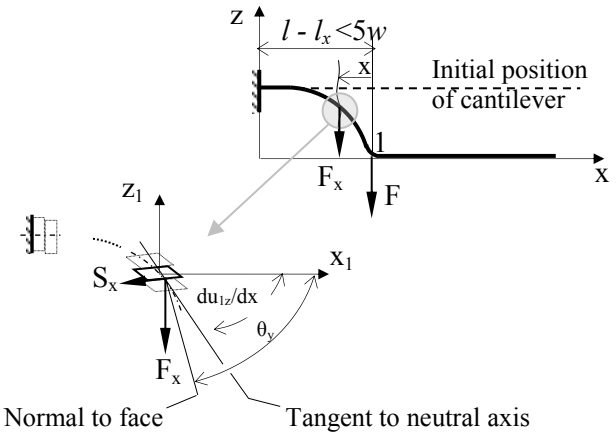

Figure 4. Microcantilever under bending and shear deformations [6, 8].

In this situation, the cross-section is no longer perpendicular to the neutral axis in the deformed state (figure 4) shearing effects produces an additional angular deformation $\theta_y(x) - \frac{\mathrm{d}u_{1z}(x)}{\mathrm{dx}}$.

The angle θ_y is determined based on:

$$\theta_y(x) = \frac{F \cdot \left[(l - l_x)^2 - x^2\right]}{2EI_y} \tag{9}$$

The equivalent stress for a cross-sectional element located to the x distance from the point 1 where the force F_x is applied can be determined using:

$$\sigma_{ech} = \sqrt{\sigma_b(x)^2 + 3\tau(x)^2} \tag{10}$$

where:

$$\tau(x) = \kappa \frac{S_x}{A} = \kappa \frac{F_x \cdot \cos\left[\theta_y(x) - \frac{\mathrm{d}u_{1z}(\mathrm{x})}{\mathrm{dx}}\right]}{w \cdot t} \tag{11}$$

$$\sigma_b(x) = \frac{6F_x \cdot (l - l_x - x)}{w \cdot t^2} \tag{12}$$

MEMS component failure as a function of the force position (figure 2), can occur in various situations: (a) fracture - where a high value force is applied close to the anchor and the shear stress becomes significant in comparison to the bending moment, and (b) excessive deformations, both elastic and plastic - when flexible plate not recover its shape after loading [6, 8].

2.2. Stiction and adhesion considerations

2.2.1. Peel number. The surface effects produce strong adhesion, friction and wear and are major problems which limit both manufacturing efficiency and lifetime of several MEMS devices [9]. It is known that adhesion is caused by capillary, electrostatic, van der Waals forces, and can also be caused by inertia (shock, rapid air flow) forces. On the other hand, stiction phenomenon is an unintentional adhesion of microstructure on the substrate when recovery forces are unable to overcome the interfacial forces. The problem of MEMS stiction can be divided into two categories: release-related stiction and in-use stiction [9]. Consequently adhesion and stiction can be a catastrophic failure that deserves attention.

We have focused on MEMS devices exposure to environment conditions when stiction phenomenon appears. Theories used in this paper are environmental theories of continuous elastic medium and therefore assume that no plastic deformation occurs.

To study the phenomenon of adhesion of mobile MEMS microstructures brought to the substrate, it was proposed by Mastrangelo and Hsu in [10], a dimensionless number, called peel number. This peel number, N_P, is the ratio of the elastic deformation energy stored in the deformed microstructure to the work of adhesion between the microstructure and the substrate. The microstructure will not join to the substrate if $N_P > 1$, more exactly the restored elastic strain energy is greater than the work of adhesion. Furthermore when $N_P \leq 1$, the deformed microstructure does not have enough energy to overcome the adhesion between the beam and the substrate.

For a long cantilever of thickness t and elastic modulus E suspended at a distance g_0 from the substrate, illustrated in figure 2, the peel number is [9, 10]:

$$N_p = \frac{3E \cdot t^3 \cdot g_0^2}{2(l - l_x)^4 \cdot \omega} \tag{13}$$

where ω is the work of adhesion between the cantilever and the substrate.

For a short cantilever beam with just its free-end adhered to the substrate, the corresponding peel number is [9, 10]:

$$N_p = \frac{3E \cdot t^3 \cdot g_0^2}{8l^4 \cdot \omega} \tag{14}$$

In this case, provided that the stored elastic strain energy is equal to the energy of adhesion, the peel number $N_P = 1$, from equation (14) could be determined the maximum dimensions of the microstructures (length of cantilever) that will not stick to the substrate:

$$l_{\max} = \left(\frac{3E \cdot t^3 \cdot g_0^2}{8 \cdot \omega} \right)^{1/4} \tag{15}$$

2.2.2. The influence of surface roughness on adhesion. The energy required of detachment the cantilever from the substrate taking into account the influence of surface roughness on adhesion could be expressed by [9]:

$$U_s = w \cdot l_x \cdot \omega' = w \cdot l_x \cdot f(\delta) \cdot \omega \tag{16}$$

Where the effective work of adhesion ω', taking into consideration the surface roughness is given by [9]: $\omega' = f(\delta) \cdot \omega$ and $f(\delta)$ is a dimensionless roughness function which reflects the influence of surface roughness on adhesion.

Elastic strain energy is [9]:

$$U_E = \frac{6E \cdot I_y \cdot g_0^2}{(l - l_x)^3} \tag{17}$$

At equilibrium $\frac{d(U_S + U_E)}{d(l - l_x)} = 0$ results the corresponding peel number for cantilever beam adhesion to a rough surface $\overline{N}_p = \frac{N_p}{f(\delta)}$. This express indicates that the adhesion of a cantilever beam with a rough substrate is reduced with increasing adhesion parameter δ [9].

3. Experimental program

3.1. Investigated sample

The investigated samples (figure 5) are microcantilevers with various geometrical dimensions made from gold (electroplated + about 40nm evaporated Au) with a Young's modulus of E = 86GPa. The structures were fabricated by LAAS laboratory in Toulouse (France) in 10 lithography and deposition steps using a wafer substrate of silicon, with a gap between flexible part and substrate of about 3μm. The geometrical dimensions of the microcantilevers are: l = 300, 350, 400, 450, 500, 550, 600, 650, 700, 750, 800μm; w = 35μm; t = 2μm.

3.2. Experimental procedure

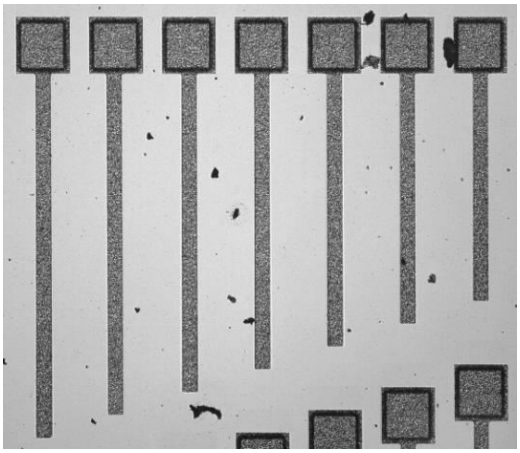

Figure 5. Samples for experimental tests.

Stiffness of investigated cantilevers is experimentally determined based on force versus deflection of the samples. Experimental-analytical evaluation of stress implies to find the experimental force that bends the flexible plate to substrate and to compute the stress by using relation (6) for long beam and relation (10) for shortest one.

Investigations were performed with an acoustic isolated and environment controlled atomic force microscope (AFM) XE 70 using the contact mode. The introduction in 1985 of the AFM based technique, due to its high spatial resolution and also force and displacement sensing capabilities is provided as a method for measuring ultra-small forces between a probe tip and an engineering surface and also has been used for morphological and surface roughness on the nanoscale, as well as for friction and adhesion measurements.

Stiction problems are typical to the electrostatic actuated MEMS cantilevers. In our experiments the electrostatic force is changed with a mechanical force performed by the bending deflection of an AFM probe with known stiffness, which deflects the samples directly to substrate. For a given deflection of investigated cantilevers, the correlation between the electrostatic force and the used mechanical one, based on equations (2) and (3), can be written as:

$$k_{AFM} \cdot z_{AFM} = \frac{\varepsilon \cdot w(l - l_x) \cdot U^2}{2(g_0 - u_z)^2} \tag{18}$$

where k_{AFM} is the stiffness of AFM probe and z_{AFM} is its bending deflection.

During tests, the position of the acting force (position of AFM probe) which bends the flexible plate to substrate is applied at the beams free-end. After, it is moved from the free-end towards the anchor. In this situation, the contact area between flexible plate and substrate increases.

The tests were performed at room temperature (22°C) and at relative humidity RH of 40%. Each measurement was repeated many times in order to improve the accuracy of the experimental results.

The cantilever used for tribological investigation in contact mode was HQ-NSC35/Hard/Al BS from Si_3N_4 with 30nm coating aluminum on the backside, with a nominal value of the spring constant k = 16Nm^{-1} and the following geometrical parameters: length 130μm, width 35μm, thickness 2μm.

During AFM tests the vertical piezoelectric displacement of the scanning head z_{piezo} is controlled and the bending deflection of AFM probe is optically monitored. The bending deflection of cantilevers can be determined as $z_{sample} = z_{piezo} - z_{AFM}$. The normal load F applied on investigated samples is the same as the force on the AFM probe that is obtained based on the bending deflection z_{AFM} and the stiffness of AFM probe as included in equation (18). Slope of the load vs. displacement experimental curve provides the stiffness of the microcantilevers. The maximum AFM force that bends the samples

to substrate is used to determine the bending stress. The spectroscopy in point is used to determine the adhesion between flexible structure and their substrate.

3.3. Stiffness and stress evaluation

3.3.1. Stiffness and stress for a force applied on the cantilevers free-end. Samples with the length between 300µm and 800µm were investigated in order to determine the influence of length on the cantilever stiffness. A mechanical AFM force was applied at the free end of each cantilever until it reached the substrate, i.e. a distance of 3µm. Based on the AFM experimental curve and the methodology described above the stiffness was obtained between between 0.28N/m for sample of 300µm length and 0.012N/m for sample of 800µm length. In figure 6 are plotted the dependence between applied force and cantilever deflection for two samples with the length of 300µm and 800µm. It is observed that as the length of samples increases, the stiffness decreases, respectively. With other words, increasing the length of the sample the force required to bend the sample to the substrate decreases.

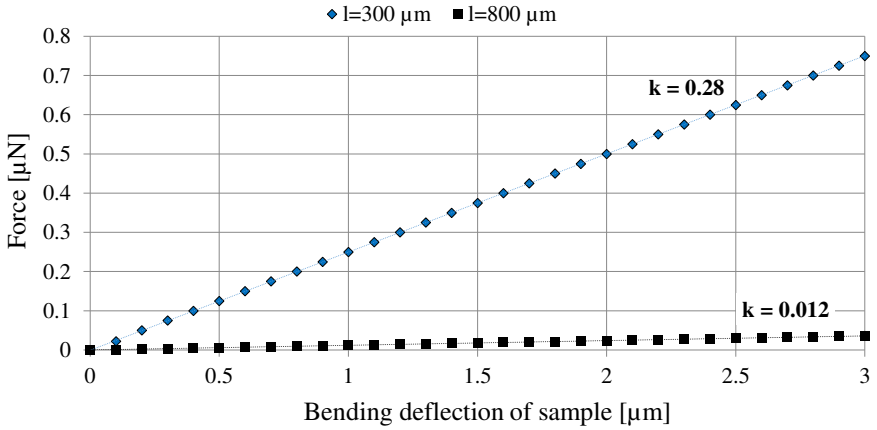

Figure 6. Experimental bending force versus deflection of samples.

The investigated cantilevers were also numerically analyzed by Finite Element (FE) method using ANSYS Workbench 13.0 software. The static structural analysis included large deflection option and uses a FE model consisting of hexahedral elements with an element size of 1.5µm. For the shortest cantilever the generated mesh has about 197000 elements and 245000 elements for the longest. Deflection under a unit load applied as in the experiment at the free end of the shortest cantilever (l = 300µm) is presented in figure 7a. Under the applied force, a bending stiffness equal to 0.2261 was numerically determined for the cantilever with a length of 300µm.

The same experimental and numerical analysis was applied for all samples and the comparative results of stiffness are presented in figure 7b. It can be observed that the stiffness decreases as the length increases. A good correlation between the stiffness obtained based on numerical analysis and experimental test is observed.

Using the experimental applied forces and the modulus of elasticity, the bending stress for different deflections positions are computed based on equation (6). Figure 8 presents the stress variation as a function of the bending deflection of the shortest and longest samples. The force was applied at the beam free-end and a good correlation between the bending stresses obtained based on numerical analysis and experimental test is observed.

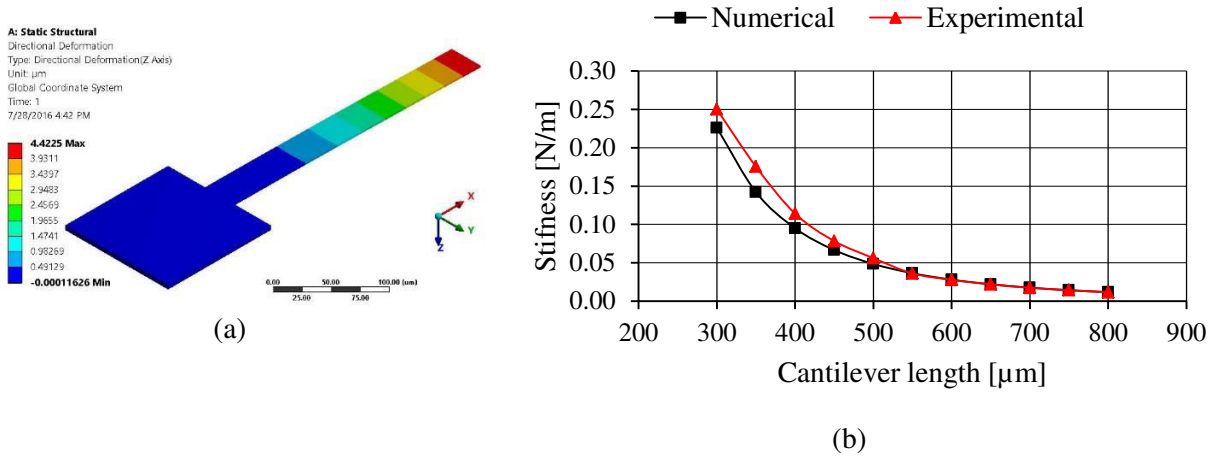

Figure 7. (a) FE analysis of the cantilever deflection with a length of 300µm, (b) Experimental and numerical bending stiffness versus the length of samples.

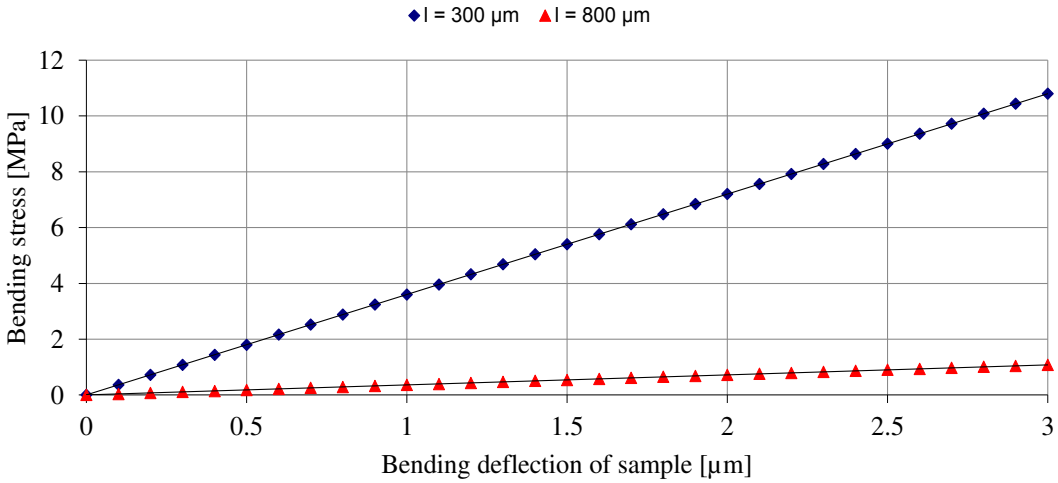

Figure 8. Bending stress versus bending deflection of samples with the lengths of 300µm and 800µm (the force acts at the free-end of cantilevers, gap = 3µm).

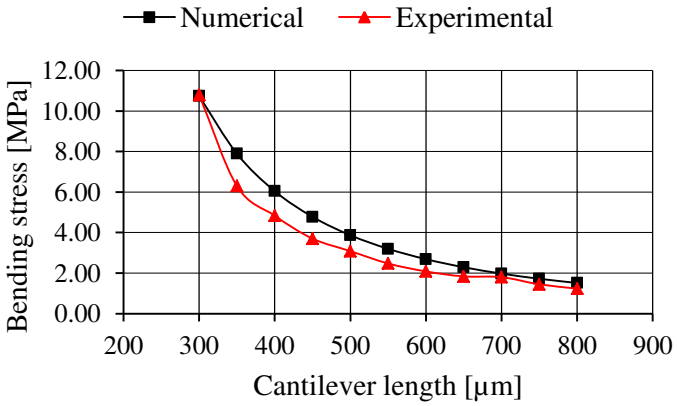

Figure 9. Experimental and numerical maximum bending stress as a function of the samples length.

The maximum bending stress at the fixed end of the microcantilever is determined for all microcantilevers with the length between 300µm and 800µm (figure 9). The same experimental and numerical analysis was applied for all samples and the comparative results of bending stress are presented in figure 9. It is observed that the bending stress decreases from 10.8MPa for the shortest sample to 1.2MPa for the sample of 800µm for the same bending deflection. On the other hand a bending stress equal by 10.742MPa was numerically determined for the cantilever with a length of 300µm and 1.512MPa for the cantilever with a length of 800µm. A good correlation between the bending stresses obtained based on numerical analysis and experimental test is observed.

3.3.2. Stiffness and stress evaluation for different force positions on a microcantilever. The experimental variation of stiffness depending on the force positions for the cantilever with the length 800µm is presented in figure 10 and the bending stresses variation of the same sample is shown in figure 11. During tests, the position of the acting force, which deflects the samples to substrate, was changed in the case of $(l - l_x) \geq 5w$. In this situation the Euler-Bernoulli beam model was considered (cross-sections remain perpendicular to the neutral axis). If we go too close to the anchor the shearing effects become important, and the regular bending deformations are augmented by the addition of shearing deformations, according to the Timoshenko's beam model.

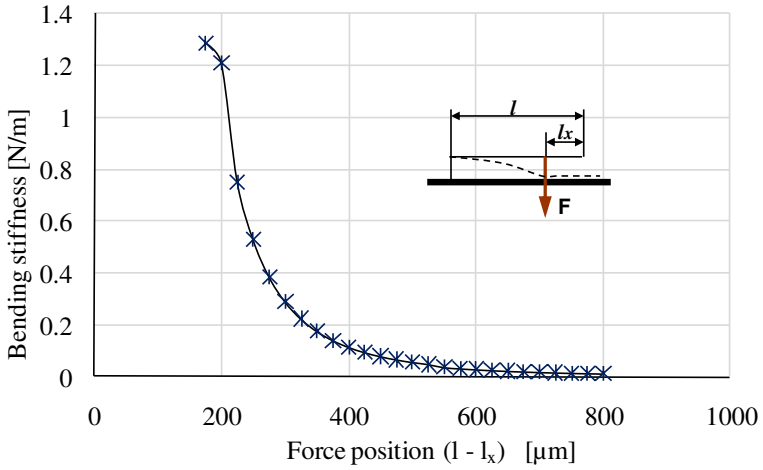

Figure 10. Experimental variations of stiffness as a function of the force positions $(l - l_x)$ on 800µm length cantilever.

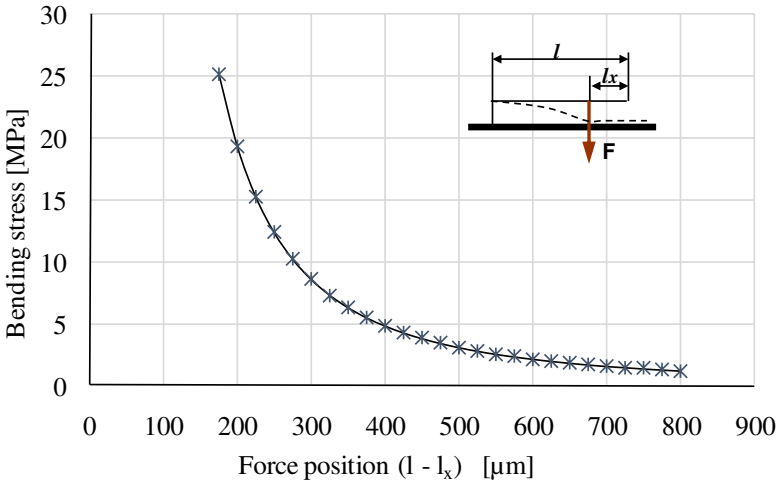

Figure 11. Experimental variations of bending stress as a function of the force positions $(l - l_x)$ of the cantilever with 800µm length.

As expected, an increase of the sample stiffness is observed as we apply a force close to the anchor.

Moreover, we can observe that, the bending stress is increasing if the force is applied close to anchor and produces sample deformation until substrate. Indeed, the stress is mainly influenced by the width *w* and thickness *t* of samples. Based on these graphs at any time we can determine the stiffness of the sample as a function of the acting electrode position as well as the maximum bending stress from structure.

3.4. Adhesion evaluation

Using AFM experimental curves, adhesion between microcantilevers and substrate can be determined. An experimental AFM curve of flexible structures has two different slopes as shown in figure 12 and figure 13. The unloading part of curve (from point 1 to 3) corresponds to the retracting of the AFM probe to its initial position. This part is used to determine the adhesion between microcantilever and substrate, phenomenon that occurs in the position 2 where the cantilever should be detached from substrate and moved to its initial position. A peak in the unloading curve can be observed in this point, and the peak height is directly proportional with the adhesion force between cantilever and substrate. The force is applied at the beam free-end. The adhesion force increases as the stiffness of samples decreases which can be seen in figure 12 for the cantilever with the length of 450µm comparatively with the sample with the length of 650µm (figure 13).

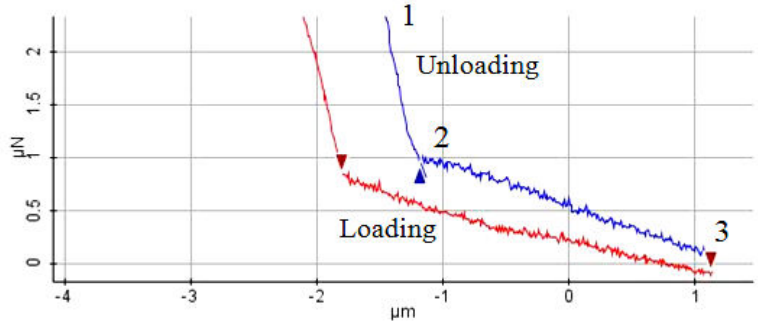

Cursors

Cursor	ΔX(µm)	ΔY(nN)	Left X(µm)	Left Y(nN)	Right X(µm)	Right Y(nN)
Trace	2.930	-916.272	-1.796	836.278	1.134	-79.994
Retrace	0.018	54.090	-1.179	945.203	-1.161	999.294

Figure 12. AFM experimental curve of a cantilever of 450µm length.

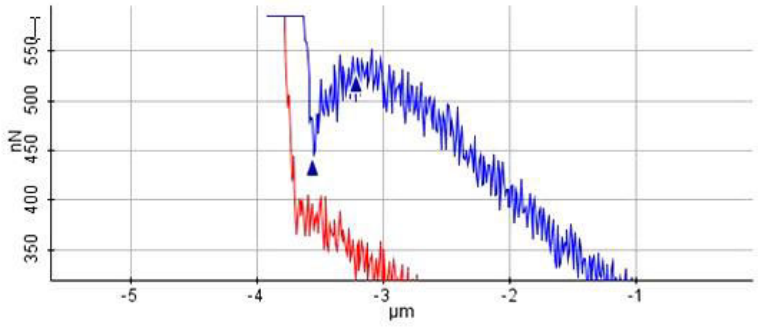

Cursors

Cursor	ΔX(nm)	ΔY(nN)	Left X(µm)	Left Y(nN)	Right X(µm)	Right Y(nN)
Trace	0.000	0.000	0.791	-46.043	0.791	-46.043
Retrace	338.982	84.147	-3.555	445.583	-3.216	529.730

Figure 13. Experimental adhesion of a cantilever of 650µm length.

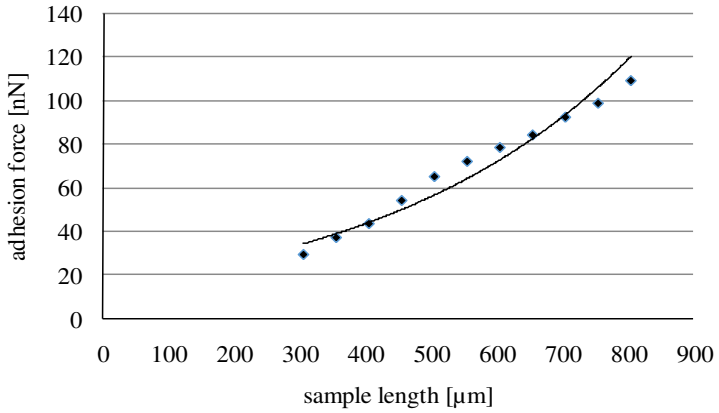

Figure 14. Experimental adhesion force versus sample length.

The same tests were performed for all investigated samples when a force is applied at the beam free-end. The variation of adhesion force obtained for the whole set of experimentally cantilevers is represented in figure 14. It is observed that the adhesion force between investigated cantilevers and substrate decreases with decreasing the length of samples. From the chart we can determine the value of adhesion force for the membrane that interests us.

4. Conclusions

The effect of geometrical dimensions (length) on mechanical and tribological behavior of MEMS cantilevers made of electroplated gold was analyzed in this paper. The force position (corresponding to the position of the acting electrode) was applied at the beams free-end and after it was moved from the cantilevers free-end towards to the anchor.

The dependences between stiffness and stress as a function of the cantilever length as well as their dependences on the variable travel range of load have been investigated. It has been experimentally determined that the cantilever stiffness decreases as the length increases, more exactly from 0.28N/m for sample of 300µm length to 0.012N/m for sample of 800µm length. Using numerical simulation a bending stiffness equal to 0.2261 was determined for the cantilever with a length of 300µm and 0.01175 for the cantilever with a length of 800µm. The numerical results are in good correlation with experimental values.

Experimental investigations have shown that deflections and stresses generated by movement of applied force towards the anchor should be analytically described using two hypotheses. For positions far from the anchor (length at least 5 times larger than the largest cross-sectional dimension) the Euler-Bernoulli beam model must be employed. For closer force positions relatively to anchor shearing effect become important and the regular bending deformations has to be corrected by the addition of shearing deformations, according to a model known as Timoshenko's beam model.

In our experiments, in order to avoid plastic deformation of cantilevers, we stopped the force position at the situation when only the Euler-Bernoulli beam model (cross-sections remain perpendicular to the neutral axis) have to be considered ($l - l_x \geq 5w$). Experimental and numerical maximum bending stresses as a function of the samples length show a very good correlation of the results.

The differences in terms of stiffness and bending stresses between the situations of separate analysis of each cantilever (the force applied at free-end) or by moving the force towards the anchor, in the same loading position, in case of the longest cantilever are small. Due to the restricted movement of the free end (friction between the cantilever and substrate) when the cantilever was deflected to the substrate a low stiffness increase can be noticed in the second analysis.

A theoretical consideration about stiction and adhesion has been presented in the paper followed by experimental test. Using the AFM experimental force versus deflection curve variation of adhesion

force for the whole set of cantilevers was obtained for a force applied to the free end of the samples. It can be stated that the adhesion force increase when the cantilever length increase. The phenomenon is mainly due to the restoring forces that depend on the stiffness value. A smaller stiffness will produce a lower restoring force. Considering the experimental results presented in the paper concerning to the adhesion effect we can determine the value of adhesion force for the cantilever that interests us. Based on experimental results obtained it is possible to appreciate the tribomechanical behavior of thin gold cantilevers when a moving force acts over the cantilever.

Acknowledgments
This work was supported by the Romanian Space Agency – STAR Project no. 97 - 2013 grant from the Research Program for Space Technology Development and Innovation and Advanced Research (STAR).

References
[1] Chuang W C Lee, H L Cang P Z and Hu Y C 2010 *Sensors* **10** 6149-6171
[2] Spearing S M 2000 *Acta Mater* **48** 179-196
[3] Abdel-Rahman E M, Younis M I and Nayfeh A H 2002 *J Micromech Microeng* **12** 759
[4] Loui A, Goericke F T, Ratto T V, Lee J, Hart B R and King WP 2008 *Sensor Actuator A- Phys* **147** 516-521
[5] Lobontiu N and Garcia E 2004 *Mechanics of microelectromechanical systems* (Boston: Springer Science & Business Media).
[6] Pustan M, Rochus V and Golinval J-C 2010 Effects of the geometrical dimensions on stress and strain of electrostatically actuated MEMS resonators at pull-in and stiction positions *Proc. IEEE Conference on Thermal, Mechanical & Multi-Physics Simulation, and Experiments in Microelectronics and Microsystems (EuroSimE)* pp. 1-5
[7] Young W C and Budynas R G 2002 *Roark's formulas for stress and strain* vol 7 (New York: McGraw-Hill)
[8] Pustan M S 2015 *Mechanical and tribological characterization of MEMS* (Hab. Thesis, Cluj Napoca) available at http://www.utcluj.ro/media/documents/2015/Teza_de_Abilitare_Pustan_Marius_1.pdf (15.06.2016)
[9] Zhao Y P, Wang L and Yu T 2003 *J Adhes Sci Technol* **17** 519-546
[10] Mastrangelo C H and Hsu C 1993 *J Microelectromech S* **2** 44-55